



## Tracking major storms from microseismic and hydroacoustic observations on the seafloor

Céline Davy, Guilhem Barruol, Fabrice R. R. Fontaine, Karin Sigloch,  
Eléonore Stutzmann

### ► To cite this version:

Céline Davy, Guilhem Barruol, Fabrice R. R. Fontaine, Karin Sigloch, Eléonore Stutzmann. Tracking major storms from microseismic and hydroacoustic observations on the seafloor. *Geophysical Research Letters*, 2014, 10.1002/2014GL062319 . hal-01236164

**HAL Id: hal-01236164**

**<https://hal.univ-reunion.fr/hal-01236164>**

Submitted on 1 Dec 2015

**HAL** is a multi-disciplinary open access archive for the deposit and dissemination of scientific research documents, whether they are published or not. The documents may come from teaching and research institutions in France or abroad, or from public or private research centers.

L'archive ouverte pluridisciplinaire **HAL**, est destinée au dépôt et à la diffusion de documents scientifiques de niveau recherche, publiés ou non, émanant des établissements d'enseignement et de recherche français ou étrangers, des laboratoires publics ou privés.



# Geophysical Research Letters

## RESEARCH LETTER

10.1002/2014GL062319

### Key Points:

- Observations of microseisms on the ocean bottom induced by a passing cyclone
- Secondary microseisms beneath the storm composed of body and Rayleigh waves
- Trackability of major storms using ocean bottom seismometers and hydrophones

### Supporting Information:

- Texts S1–S3 and Figure S1
- Movie S1
- Movie S2

### Correspondence to:

C. Davy and G. Barruol,  
celine.davy@univ-reunion.fr;  
guilhem.barruol@univ-reunion.fr

### Citation:

Davy, C., G. Barruol, F. R. Fontaine, K. Sigloch, and E. Stutzmann (2014), Tracking major storms from microseismic and hydroacoustic observations on the seafloor, *Geophys. Res. Lett.*, 41, doi:10.1002/2014GL062319.

Received 23 OCT 2014

Accepted 3 DEC 2014

Accepted article online 11 DEC 2014

## Tracking major storms from microseismic and hydroacoustic observations on the seafloor

Céline Davy<sup>1</sup>, Guilhem Barruol<sup>1</sup>, Fabrice R. Fontaine<sup>1</sup>, Karin Sigloch<sup>2,3</sup>, and Eléonore Stutzmann<sup>4</sup>

<sup>1</sup>Laboratoire GéoSciences Réunion, Université de La Réunion, Institut de Physique du Globe de Paris, Sorbonne Paris Cité, UMR CNRS 7154, Université Paris Diderot, Saint Denis CEDEX 9, France, <sup>2</sup>Earth Sciences Department, University of Oxford, Oxford, UK, <sup>3</sup>Department of Earth and Environmental Sciences, Ludwig-Maximilians-Universität München, Munich, Germany, <sup>4</sup>Institut de Physique du Globe de Paris, Sorbonne Paris Cité, UMR 7154 CNRS, Paris, France

**Abstract** Ocean wave activity excites seismic waves that propagate through the solid earth, known as microseismic noise. Here we use a network of 57 ocean bottom seismometers (OBS) deployed around La Réunion Island in the southwest Indian Ocean to investigate the noise generated in the secondary microseismic band as a tropical cyclone moved over the network. Spectral and polarization analyses show that microseisms strongly increase in the 0.1–0.35 Hz frequency band as the cyclone approaches and that this noise is composed of both compressional and surface waves, confirming theoretical predictions. We infer the location of maximum noise amplitude in space and time and show that it roughly coincides with the location of maximum ocean wave interactions. Although this analysis was retrospectively performed, microseisms recorded on the seafloor can be considered a novel source of information for future real-time tracking and monitoring of major storms, complementing atmospheric, oceanographic, and satellite observations.

Texte

## 1. Introduction

Storms over the oceans represent major sources of microseismic noise, which travels through the solid earth and is recorded worldwide by broadband seismometers. Microseismic noise is classically divided into primary and secondary microseisms, which are excited by different physical processes. Primary microseisms have the same periods as ocean swells (between 8 and 20 s) and are accepted to be generated through direct interaction of swell-induced pressure variation with the sloping seafloor in coastal areas [e.g., Hasselmann, 1963; Barruol *et al.*, 2006]. Secondary microseisms, which dominate seismic noise worldwide, have half the period of ocean waves (typically between 3 and 10 s) and are thought to be induced by depth-independent, second-order water pressure fluctuations on the seafloor, which are generated by the interference of swells of similar periods that travel in opposite directions [Longuet-Higgins, 1950].

The oceanic source regions of secondary microseisms have been remotely detected and located using terrestrial seismic networks [e.g., Obrebski *et al.*, 2012] and techniques such as beamforming [e.g., Landès *et al.*, 2010] or polarization analyses [e.g., Schimmel *et al.*, 2011]. They are clearly associated with winter storms in both hemispheres [e.g., Ardhuin *et al.*, 2011; Reading *et al.*, 2014] and have been numerically modeled [e.g., Stutzmann *et al.*, 2012; Gualtieri *et al.*, 2014]. A few observations of storms have already been achieved either by individual seismometers on the seafloor [e.g., Latham *et al.*, 1967; Chi *et al.*, 2010] or by small-scale ocean bottom seismometer (OBS) networks [e.g., Lin *et al.*, 2014]. Here we present the first investigation of secondary microseismic noise recorded on the seafloor by a large-scale, broadband seismological network while a cyclone was passing over it. Major tropical summer storms of this kind form over the oceans and are called “cyclones” in the Indian Ocean, “hurricanes” in the Atlantic, and “typhoons” in the Asian Pacific.

## 2. The Ocean Bottom Network of the Réunion Hotspot and Upper Mantle–Réunions Unterer Mantel Project

The French-German RHUM-RUM (Réunion Hotspot and Upper Mantle–Réunions Unterer Mantel) project [Barruol and Sigloch, 2013] deployed 57 broadband ocean bottom stations at 2500 to 5400 m depth and over an area of 2000 × 2000 km<sup>2</sup>, centered on La Réunion Island (Figure 1). From their deployment in October–November 2012, the ocean bottom stations recorded autonomously and were retrieved during a

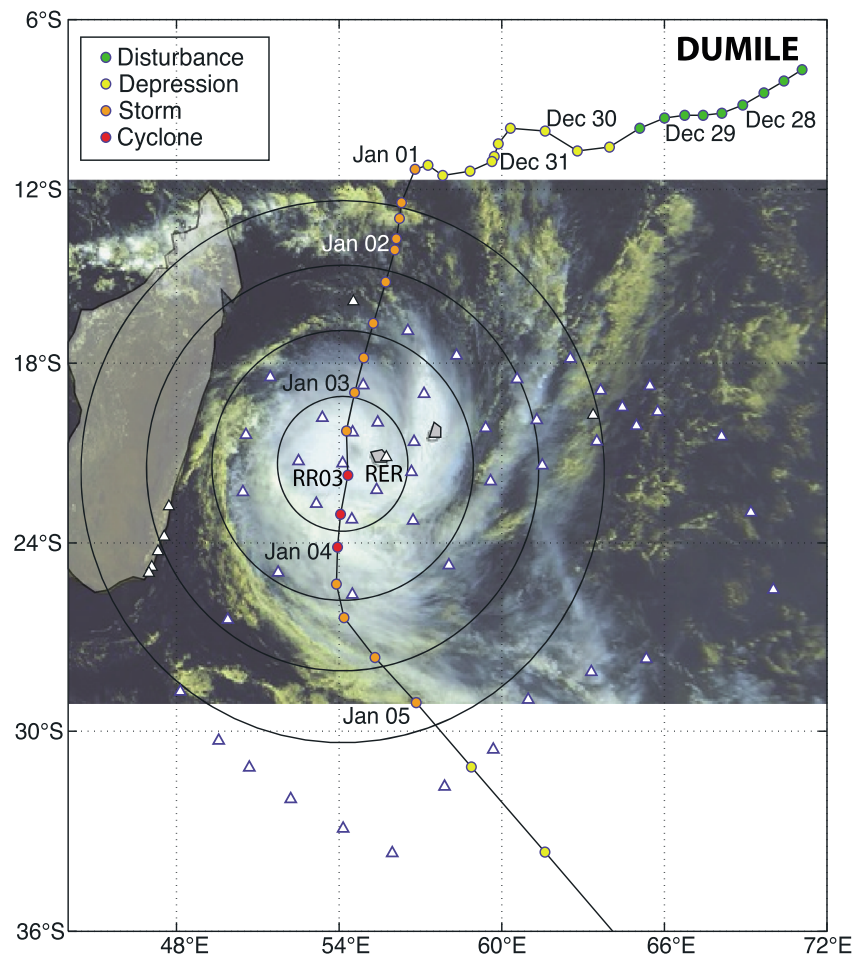


**Figure 1.** Ocean bottom seismic network and the cyclone Dumile. Meteosat-9 satellite image of Dumile on 3 January 2013 at 08:15 UTC (credits: “Météo-France–Centre de météorologie spatiale”). Superimposed are the station locations: the blue triangles indicate the 57 broadband OBS locations in the RHUM-RUM network; the black triangles are terrestrial stations, including permanent Geoscope station RER on La Réunion Island. The four concentric circles indicate the distances of 250, 500, 750, and 1000 km from OBS station RR03. The colored circles map the trajectory of the storm center in 6 h increments, as it passes through various categories of meteorological intensity.

recovery cruise in October–December 2013. The 57 stations were equipped with broadband, three-component seismometers (corner frequencies of 60, 120, or 240 s and sampling rates of 50–100 Hz), and with broadband hydrophones (corner period 100 s, cutoff frequency 8 Hz, and sampling rates of 50–100 Hz). For details on instrumentation, see the supporting information.

During the yearlong recording period, the southwestern Indian Ocean suffered seven tropical cyclones, of which cyclone “Dumile” (further characterized in the supporting information) was the only one to pass directly over our seismic network in Figure 1. This configuration provides the unique opportunity for investigation of (i) the storm-generated water pressure fluctuations that propagate from sea surface to seafloor, (ii) the solid earth displacement excited by these water pressure fluctuations on the seafloor, (iii) the nature of the seismic waves that propagate away from the excitation area, and (iv) the trackability of the cyclone from seismic observations for future real-time monitoring.

### 3. Microseisms Generated by the 2013 Tropical Cyclone Dumile

For the time period covering the cyclone’s approach and passage (28 December 2012 to 6 January 2013), we analyzed records from broadband ocean bottom seismometers and their co-located hydrophones. Raw waveforms were detrended, windowed by a 5% Hanning taper, and transferred to ground displacement by

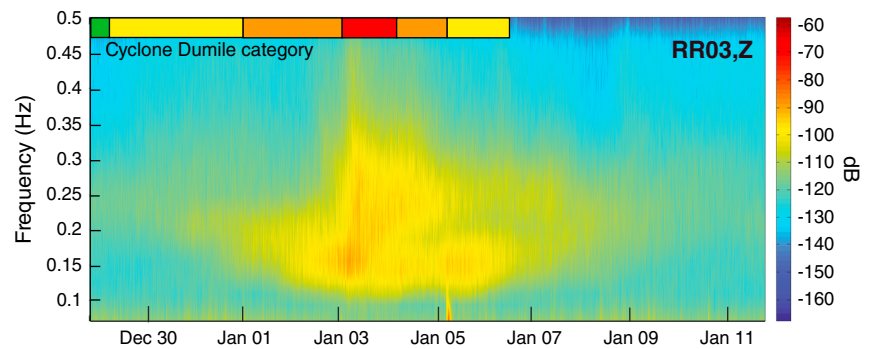


**Figure 2.** Spectrogram of vertical ground displacement on the seafloor during cyclone Dumile. Time-frequency distribution of seismic noise power (in decibel with respect to acceleration) on the vertical component of OBS RR03 between 29 December 2012 and 11 January 2013. Storm category is indicated by the color bar at the top, using the same colors as in Figure 1.

deconvolution with the instrument response. Figure 2 shows a spectrogram of vertical ground displacement at RR03, an exemplary ocean bottom station on the storm track. Seismic power was clearly elevated during the days when the cyclone passed directly overhead (on 3 January; Figure 1) and was concentrated in the frequency range between 0.1 and 0.35 Hz, which is the secondary microseismic noise band.

We determined the absolute noise amplitudes on moving time windows of 1 h duration, to which we applied a Butterworth band-pass filter (second order, corner frequencies at 0.1 Hz and 0.35 Hz). The hourly root-mean-square (RMS) values of these amplitudes, obtained for various instrument locations and components, are shown in Figure 3. At most OBS, RMS amplitude variations follow trends similar to the example of OBS RR03 (Figure 3a). While the cyclone was still more than 1300 km away (28–31 December), the ambient seismic noise on the horizontal components ( $x$  and  $y$ ) dominated that on the vertical component ( $z$ ). Horizontal ground motion shows a clear tidal signature [Crawford and Webb, 2000; Fontaine *et al.*, 2014], with two high tides per day, and amplitudes up to  $2\ \mu\text{m}$ , while the level on the vertical component is stable around  $0.5\ \mu\text{m}$ . As the cyclone approached to within 1300 to 500 km distance, the amplitude on the vertical component rose above the amplitude on the two horizontals. At distances below 300 km (3 January), the amplitudes on all components dramatically increased. Displacement reached  $4\ \mu\text{m}$  on the horizontal components and up to  $8\ \mu\text{m}$  on the vertical component. During the whole storm passage, pressure variations measured by the hydrophone closely followed the vertical ground displacement. The high correlation coefficient ( $>0.99$ ) computed on 24 h long windows between the hydrophone and the vertical RMS amplitudes at OBS RR03 from 1 to 4 January suggests that at least part of the secondary microseisms (namely, the vertical ground displacement) is caused by water pressure fluctuations on the seabed. Such an excitation mechanism was proposed by Longuet-Higgins [1950], who demonstrated that water pressure fluctuations beneath standing ocean waves (created by two swells of similar periods traveling in opposite directions) should have twice the frequency of their exciting swells and should be proportional in amplitude to the product of the two swell amplitudes. Compressional waves thus generated on the seabed would be extremely small compared to the surficial water waves that excite them but large enough to be recorded by seismometers. This excitation hypothesis by Longuet-Higgins [1950] is directly supported by the high correlation between water pressure and seafloor vertical ground RMS amplitude that we observe during the days when the cyclone passes over it.

#### 4. Analysis of Ground Motion Polarization

To further investigate the process of microseismic noise excitation and the nature of the seismic waves, we performed a polarization analysis in the 0.1–0.3 Hz frequency band, on 4 min long moving windows of the continuous three-component seismic data. For each window, we quantified the shape of the ellipsoid characterizing the ground motion by calculating the degree of rectilinearity of particle motion in 3-D ( $CLin$ ) and in the horizontal ( $CpH$ ) and vertical ( $CpZ$ ) planes, as well as the apparent incidence angle ( $Vpol$ ) of the ground motion [Fontaine *et al.*, 2009] (see details in the supporting information). The polarization measured at OBS RR03 before the cyclone's arrival (Figure 3c) confirms the dominant tidal signature, with a 12 h period

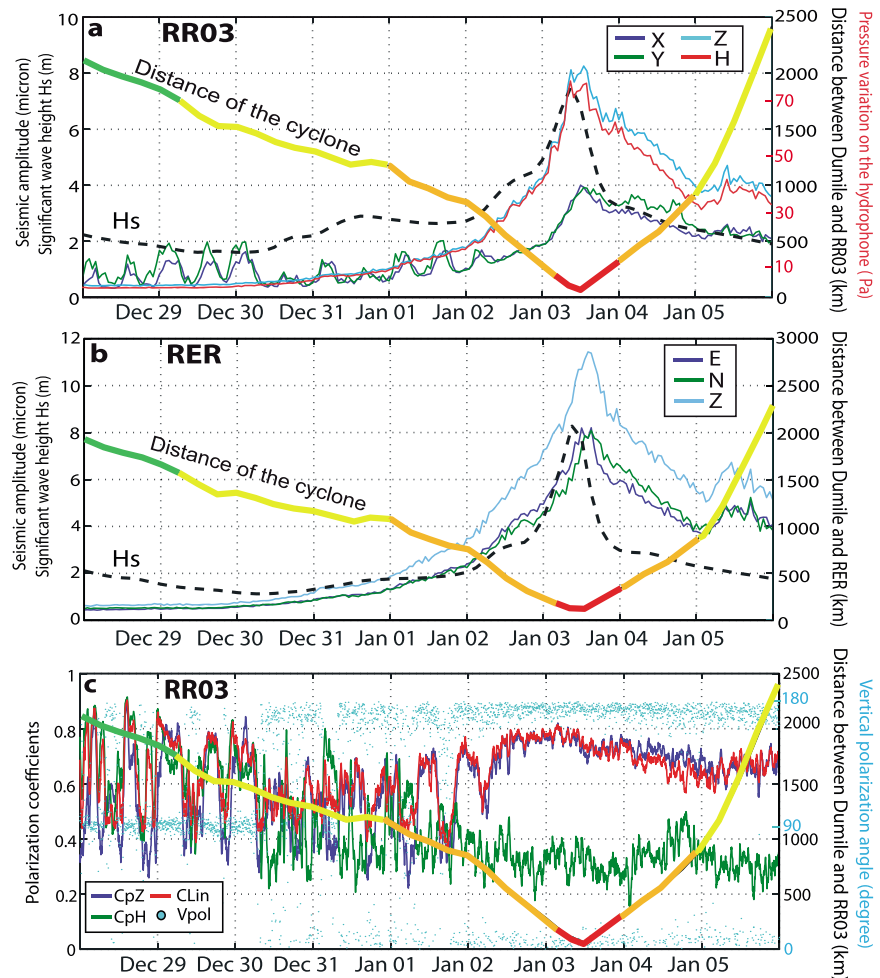


**Figure 3.** Seismic wave amplitudes in the frequency range of 0.1–0.35 Hz and polarizations during the passage of cyclone Dumile. (a) Seismic RMS amplitudes over time at ocean bottom station RR03. Ground displacement on the two horizontal (x and y) and the vertical (z) seismometer components in microns (y axis on the left side), together with water pressure variations on the hydrophone (H) in pascal (y axis on the right). The multicolored line indicates the distance of RR03 to the meteorologically determined storm center, where storm category is identified by the same colors as in Figures 1 and 2. The dashed line shows the significant ocean wave height at the sea surface in meters (y scale on the left), as predicted by NOAA's WaveWatchIII model [Tolman and Chalikov, 1996]. (b) Seismic RMS amplitudes over time at island station RER. Ground displacement on the two horizontal (E and N) and the vertical (z) seismometer components in microns (y axis on the left side). Dashed line: NOAA's WaveWatchIII model predicted Hs. Distance from the storm center, storm category, and significant wave height are shown as in Figure 3a. (c) Polarization of ground displacement over time at ocean bottom station RR03. Vertical (CpZ), horizontal (CpH), and rectilinear (CLin) polarization coefficients were computed in moving time windows of 4 min duration. The light blue dots show the vertical polarization angle (Vpol) in degrees, each dot corresponding to one 4 min window. The 0° or 180° indicates mostly vertically polarized ground displacement, whereas 90° indicates horizontal motion. Distance from the storm center and storm category are superimposed, as shown in Figures 3a and 3b.

variation of the polarization parameters (CpZ, CpH, and CLin), and horizontal ground motion prevailing ( $Vpol \sim 90^\circ$ ) [Crawford and Webb, 2000]. The polarization coefficients stabilize on 2 January around 12:00 UTC, at a station-cyclone distance of about 500 km. Over the following 2 days, as Dumile passes over the station, we predominantly observe vertical polarization ( $CpZ > 0.75$ ,  $CLin > 0.75$ , and  $Vpol \sim 0^\circ$  or  $180^\circ$ ). Interestingly, the values of  $CLin > 0.75$  observed at RR03 are much higher than those observed at the nearby terrestrial station RER on La Réunion Island ( $CLin < 0.5$ ). This confirms that the dominant vertical ground motion observed on the seafloor beneath the storm is directly induced by compressional waves in the water column.

In addition to the body wave analysis described above, we also detected Rayleigh waves associated to the cyclone activity: in the time-frequency domain, we quantified the number of elliptically polarized signals in



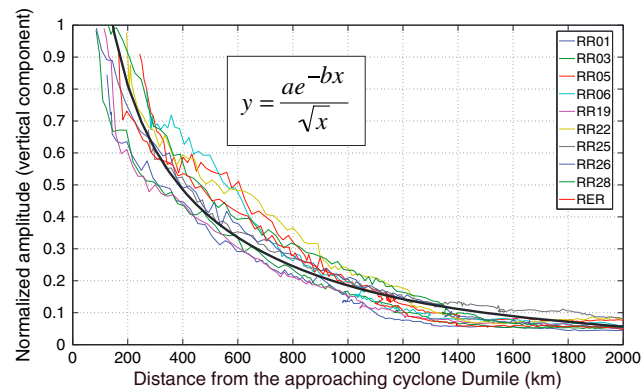


**Figure 4.** Evolution of the microseismic noise amplitude as a function of distance from the storm center. Normalized RMS amplitude of the vertical component of various OBS, located within 250 km of station RR03. They all detect the cyclone as it reaches a distance of  $\sim 1300$  km. The black curve is the mean of the best fitting equations computed for all these stations.

the vertical plane, corresponding to Rayleigh waves [Schimmel and Gallart, 2004; Schimmel et al., 2011]. Interestingly, at both OBS and terrestrial stations, we observed dominant frequencies of these elliptically polarized signals around 0.15 Hz (i.e., within the microseismic noise band) and an increase in the number of elliptical signal detections as the cyclone approaches, suggesting that Rayleigh waves are generated in the vicinity of the cyclone. The number of elliptically polarized signals detected in the frequency band between 0.1 and 0.3 Hz started to dramatically increase and remained high as long as the cyclone was closer than 1000 km.

These two analyses show that the seafloor beneath Dumile is affected by both vertical compressional and Rayleigh waves. This is in good agreement with remote observations of  $P$  wave sources associated with storms [e.g., Gerstoft et al., 2008] but also of elliptically polarized Rayleigh waves dominating the secondary microseismic noise recorded by distant land stations [e.g., Obrebski et al., 2012].

The presence of body and surface waves associated with cyclone Dumile is also consistent with numerical models [Gualtieri et al., 2014], which predict that each swell interaction acts as a source at the sea surface, radiating compressional waves through the water column. This generates  $P$  waves directly beneath the source, and surface waves at increasing distances from the storm source, by the combined effect of wave reflection and refraction on the seafloor. In the case of a tropical cyclone, which can extend over more than 1000 km laterally (Figure 1) and propagates at up to 25 km/h, the number, sizes, locations, and velocity of the effective microseismic source areas are unknown. This may explain why the ocean bottom seismometers located near the cyclone track simultaneously record compressional waves, as expected directly beneath a pressure source, but also surface waves, which are expected at some distance, due to lateral wave propagation away from the vertical source.

## 5. Early Detection of Tropical Cyclone Dumile

Normalized microseismic RMS amplitudes on the OBS network show a clear cyclone signal, i.e., rising noise level in the secondary microseismic band, starting at a storm-station distance of about 1300 km (Figure 4). This distance versus noise curve looks very similar for stations shown in Figure 4, all located within 250 km distance from OBS RR03 and thus from the cyclone track. As the storm approaches, the normalized amplitudes consistently rise in the network. The amplitude fits the equation used by Battaglia and Aki [2003]:  $y = (ae^{-bx})/\sqrt{x}$ , where  $x$  is the distance from the cyclone,  $a = 13.58$ , and  $b = 0.00084$ . Due to the small value for  $b$ , the dominant term is  $1/\sqrt{x}$  and reflects the amplitude decrease by geometric spreading of surface waves. Observations of microseismic noise variation across the entire OBS network during the cyclone show that the maximum absolute noise level recorded at a station primarily depends on how close the storm passes by (Figure S1 in the supporting information): if the storm remains at a distance exceeding 1250 km, the maximum noise remains small ( $< 4 \mu\text{m}$ ), whereas large noise levels ( $> 8 \mu\text{m}$ ) are observed only at stations passed by the cyclone at less than 800 km distance. The maximum noise level also depends on the storm's intensity: seismic noise amplitudes during the depression stage are low, while the largest amplitudes are observed during the cyclone phase.

Overall noise amplitude is clearly controlled by cyclone trajectory and intensity, but we also observed variations in energy partitioning between the horizontal and vertical components. For 55% of the OBS, the noise recorded on the vertical component is clearly dominant during the cyclone stage, as shown for OBS RR03, whereas for 20% of the OBS, the noise is stronger on the horizontal components. The remaining OBS show similar noise intensity on the three components. Interestingly, the ratio between the vertical and

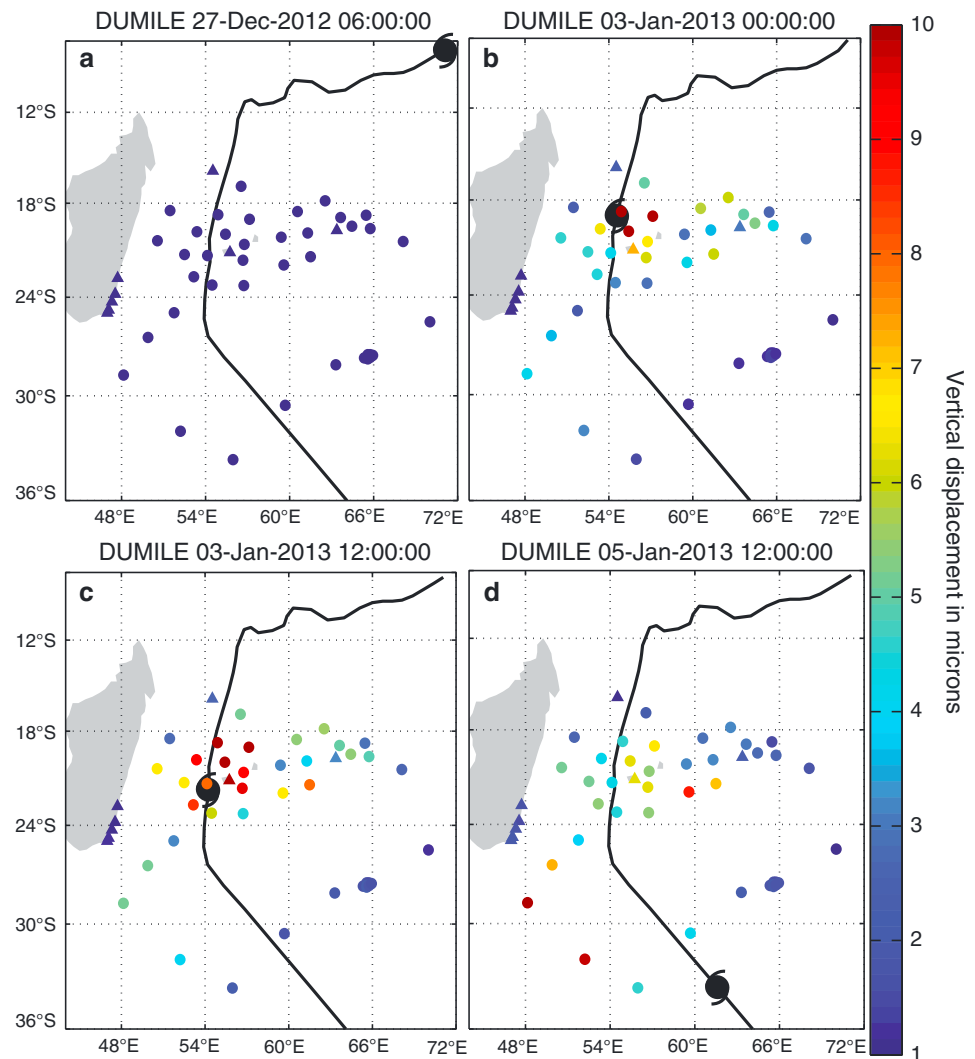


**Figure 5.** Spatiotemporal evolution of microseismic noise levels on the ocean bottom seismometers during cyclone Dumile. RMS amplitudes of the absolute vertical ground displacement (in micron) at the OBS (circles) and terrestrial stations (triangles). The color indicates noise amplitude, with a color bar saturating below 1  $\mu\text{m}$  (blue) and above 10  $\mu\text{m}$  (red). The black line shows the cyclone track, and the black circle shows the location of the cyclone center (a) on 27 December at 06:00 UTC, before the cyclone; (b) on 3 January at 00:00 UTC, at the meteorological peak of storm intensity (cyclone stage); (c) on 3 January at 12:00 UTC; and (d) on 5 January at 12:00 UTC, toward the end of cyclone passage.

horizontal components at a given OBS is roughly constant from one cyclone to another (we observed seven storms in total). This suggests that vertical/horizontal energy partitioning is partly a site effect, likely depending on shallow subsurface properties such as the thickness and the elastic parameters of the sedimentary layer [e.g., Tanimoto and Rivera, 2005].

## 6. Tracking Cyclones From Ocean Bottom Seismic Observations

Although the data were not processed in real time, analysis of the continuous time series provides time-lapse images of cyclone-induced noise amplitudes across the network from which we can infer the progression of the cyclone over the Earth's surface (Figure 5 and Movies S1 and S2 in the supporting information). Qualitatively, the hourly variations of RMS amplitude on the vertical components, normalized as in Figure 4, show an increase in noise level across the whole network as the cyclone approaches (Movie S1 in the supporting information). Even the easternmost stations, located more than 1000 km from the storm track, record the cyclone activity. In a more quantitative way (Figure 5 and Movie 2 in the supporting information), the absolute noise amplitude variations permit to locate and follow the source region of the microseisms

over time. Although the distance between stations (200 km on average) is a limiting factor in our ability of accurately locating the noise sources, we observe that the area of maximum noise is located in the vicinity of the cyclone center, as defined by Météo France from satellite images. The “seismological eye” of the microseismic noise appears to be offset 200 km to the northeast from the meteorological eye of the cyclone, which suggests that the location of maximum ocean wave interactions is located northeast of the meteorological cyclone eye. This is plausible, since a cyclone that turns clockwise in the Southern Hemisphere and propagates southward is suspected to shore up the highest waves northeast of its center, where propagation and rotation direction add up constructively.

## 7. Conclusions

Our network of 57 broadband ocean bottom seismometers in the southwestern Indian Ocean enabled the investigation of secondary microseisms on the seafloor beneath the 2013 tropical cyclone Dumile. Polarization analyses reveal that the corresponding ground motion contains both vertically polarized *P* waves and elliptically polarized Rayleigh waves. This is consistent with theoretical predictions [Longuet-Higgins, 1950], modeling [Gualtieri et al., 2014], and teleseismic observations [e.g., Gerstoft et al., 2008]. We showed that ocean bottom seismometers detect a rise in storm-generated noise levels at storm-station distances exceeding 1000 km and can be used to locate the cyclone center with good accuracy. By such retrospective analysis, we have demonstrated that microseismic noise represents a good proxy for observing the development and movement of oceanic storms. Once ocean bottom seismograms become available in real time, this approach could be used for real-time monitoring and tracking of major storms over the oceans.

## Acknowledgments

OBS data used in this work will be available at the French RESIF archive center (<http://portal.resif.fr/>). RHUM-RUM ([www.rhum-rum.net](http://www.rhum-rum.net)) is funded by the ANR (Agence Nationale de la Recherche) in France (project ANR-11-BS56-0013) and by the Deutsche Forschungsgemeinschaft in Germany, with additional support from Centre National de la Recherche Scientifique–Institut National des Sciences de l’Univers, Terres Australes et Antarctiques Françaises, Institut Polaire Paul Emile Victor, and Alfred Wegener Institut Bremerhaven. We thank the DEPAS German instruments pool for amphibian seismology hosted by AWI and the CNRS-INSU for providing the OBS. We gratefully acknowledge the crews of research vessels “Marion Dufresne” and “Meteor” for the skillful deployment and recovery of the ocean bottom sensors, the Geoscope seismological network for operating station RER, and Météo France for providing the quantitative cyclone data. We thank M. Schimmel for providing the software for the surface wave analyses. This is IGP contribution 3592.

The Editor thanks Anya Reading and an anonymous reviewer for their assistance in evaluating this paper.

## References

- Ardhuin, F., E. Stutzmann, M. Schimmel, and A. Mangeney (2011), Ocean wave sources of seismic noise, *J. Geophys. Res.*, **116**, C09004, doi:10.1029/2011JC006952.
- Barruol, G., and K. Sigloch (2013), Investigating La Réunion hot spot from crust to core, *Eos Trans. AGU*, **94**, 205–207, doi:10.1002/2013EO230002.
- Barruol, G., D. Reymond, F. R. Fontaine, O. Hyvernaud, V. Maurer, and K. Maamaatuaiahutapu (2006), Characterizing swells in the southern Pacific from seismic and infrasonic noise analyses, *Geophys. J. Int.*, **164**(3), 516–542, doi:10.1111/J.1365-246X.2006.02871.x.
- Battaglia, J., and K. Aki (2003), Location of seismic events and eruptive fissures on the Piton de la Fournaise volcano using seismic amplitudes, *J. Geophys. Res.*, **108**(B8), 2364, doi:10.1029/2002JB002193.
- Chi, W., W. Chen, B. Kuo, and D. Dolenc (2010), Seismic monitoring of western Pacific typhoons, *Mar. Geophys. Res.*, **31**(4), 239–251, doi:10.1007/s11001-010-9105-x.
- Crawford, W. C., and S. C. Webb (2000), Identifying and removing tilt noise from low-frequency (<0.1 Hz) seafloor vertical seismic data, *Bull. Seismol. Soc. Am.*, **90**(4), 952–963, doi:10.1785/0119990121.
- Fontaine, F. R., G. Barruol, B. L. N. Kenneth, G. H. R. Bokelmann, and D. Reymond (2009), Upper mantle anisotropy beneath Australia and Tahiti from P-wave polarization: Implication for real-time earthquake location, *J. Geophys. Res.*, **114**, B03306, doi:10.1029/2008JB005709.
- Fontaine, F. R., G. Roult, L. Michon, G. Barruol, and A. Di Muro (2014), The 2007 eruptions and caldera collapse of the Piton de la Fournaise volcano (La Réunion Island) from tilt analysis at a single very broadband seismic station, *Geophys. Res. Lett.*, **41**, 2803–2811, doi:10.1002/2014GL059691.
- Gerstoft, P., P. Shearer, N. Harmon, and J. Zhang (2008), Global P, PP, and PKP wave microseisms observed from distant storms, *Geophys. Res. Lett.*, **35**, L23306, doi:10.1029/2008GL036111.
- Gualtieri, L., E. Stutzmann, V. Farra, Y. Capdeville, M. Schimmel, F. Ardhuin, and A. Morelli (2014), Modelling the ocean site effect on seismic noise body waves, *Geophys. J. Int.*, **197**(2), 1096–1106, doi:10.1093/gji/ggu042.
- Hasselmann, K. (1963), A statistical analysis of the generation of microseisms, *Rev. Geophys.*, **1**, 177–210, doi:10.1029/RG001i002p00177.
- Landès, M., F. Hubans, N. M. Shapiro, A. Paul, and M. Campillo (2010), Origin of deep ocean microseisms by using teleseismic body waves, *J. Geophys. Res.*, **115**, B05302, doi:10.1029/2009JB006918.
- Latham, G. V., R. S. Anderson, and M. Ewing (1967), Pressure variations produced at ocean bottom by hurricanes, *J. Geophys. Res.*, **72**, 5693–5704, doi:10.1029/JZ072i022p05693.
- Lin, J., T. Lee, H. Hsieh, Y. Chen, Y. Lin, H. Lee, and Y. Wen (2014), A study of microseisms induced by typhoon Nanmadol using ocean-bottom seismometers, *Bull. Seismol. Soc. Am.*, **104**(5), 2412–2421, doi:10.1785/0120130237.
- Longuet-Higgins, M. S. (1950), A theory of the origin of microseisms, *Philos. Trans. R. Soc. London, Ser. A*, **243**, 1–35.
- Obrebski, M. J., F. Ardhuin, E. Stutzmann, and M. Schimmel (2012), How moderate sea states can generate loud seismic noise in the deep ocean?, *Geophys. Res. Lett.*, **39**, L11601, doi:10.1029/2012GL051896.
- Reading, A. M., K. D. Koper, M. Gal, L. S. Graham, H. Tkalčić, and M. A. Hemer (2014), Dominant seismic noise sources in the Southern Ocean and West Pacific, 2000–2012, recorded at the Warramunga Seismic Array, *Geophys. Res. Lett.*, **41**, 3455–3463, doi:10.1002/2014GL060073.
- Schimmel, M., and J. Gallart (2004), Degree of polarization filter for frequency-dependent signal enhancement through noise suppression, *Bull. Seismol. Soc. Am.*, **94**(3), 1016–1035.
- Schimmel, M., E. Stutzmann, F. Ardhuin, and J. Gallart (2011), Polarized Earth’s ambient microseismic noise, *Geochem. Geophys. Geosyst.*, **12**, Q07014, doi:10.1029/2011GC003661.
- Stutzmann, E., F. Ardhuin, M. Schimmel, A. Mangeney, and G. Patau (2012), Modelling long-term seismic noise in various environments, *Geophys. J. Int.*, **191**(2), 707–722, doi:10.1111/j.1365-246X.2012.05638.x.
- Tanimoto, T., and L. Rivera (2005), Prograde Rayleigh wave particle motion, *Geophys. J. Int.*, **162**(2), 399–405, doi:10.1111/j.1365-246X.2005.02481.x.
- Tolman, H. L., and D. Chalikov (1996), Source terms in a third-generation wind wave model, *J. Phys. Oceanogr.*, **26**(11), 2497–2518, doi:10.1175/1520-0485(1996)026<2497:stiatg>2.0.co;2.